Science of Sintering, **53** (2021) 519-534

https://doi.org/10.2298/SOS2104519K

UDK: 543.42; 546.271

Impedance Spectroscopy Studies on Steatite with B_2O_3 Ceramics Materials from Algerian Palygorskite

K. Khalfaoui[1*)], K. Boumchedda[1], A. Chaouchi[2], M. Saidi[2], N. Lamrani[2], R. Djafar[1]

[1]Research Unit Materials, Processes and Environment (UR-MPE), Faculty of Technology, University M'Hamed Bougara, Boumerdes, 35000, Algeria

[2]Laboratory of Applied Chemistry and Chemical Engineering, Mouloud Mammeri University, Tizi-Ouzou, 15000, Algeria

Abstract:

B_2O_3 was used to reduce the sintering temperature of steatite (named MSB) dielectric ceramics. Electrical properties of this composition have been studied using impedance spectroscopic method to get better understanding of the electrical conduction, dielectric relaxation mechanism, and microstructure –electrical properties relationship of the materials as a function of temperature and frequency. These samples were prepared by a solid-state reaction technique and their single phase formation was confirmed by the X-ray diffraction technique. Dielectric and complex impedance spectroscopic studies were carried out in a wide frequency (102-106 Hz) and temperature (30-500^oC) range. The dielectric constants decrease with increasing frequency for each sample, and then stabilize at frequencies lower than 100 kHz. The dielectric constant increases with the addition of B_2O_3. The nature of frequency dependence of ac conductivity of MSB follows the Jonscher power law and calculated DC conductivity follows Arrhinius behavior. The Nyquist plot (Z" vs Z') revealed the presence only of the grain boundary effect from 350^oC onwards. The occurrence of single arc in the complex modulus spectrum of MSB compositions confirms the single-phase characteristics, and also confirms the presence of non-Debye type of multiple relaxations in the material.

***Keywords**: Palygorskite; Steatite; B_2O_3; Dielectric properties; AC impedance spectroscopy.*

1. Introduction

As a general class of dielectric, steatite ceramics are inorganic materials made from natural raw materials widely available throughout the world [1-3], containing predominantly magnesium silicate and can be considered in place of alumina as a cost-effective way to meet performance requirements. After sintering, crystals of magnesium metasilicate ($MgSiO_3$) are obtained which are embedded in a vitreous matrix composed of various elements: Na, K, Fe, Al. The structure of steatite phase consists of about 70 % of crystalline $MgSiO_3$ (so-called protoenstatite) and of about 30% of glass phase [4].

Its elaboration is typical of that of porcelain allows the glass to stabilize the protoenstatite crystals crystallized at high temperature and thus avoids the polymorphic transformations of magnesium metasilicate which are accompanied by large changes in the volume of the crystalline cells, and which often leads to the appearance of microcracks in the

*) **Corresponding author:** k.khalfaoui@univ-boumerdes.dz

body of ceramics. The pure crystals of magnesium metasilicate ($MgSiO_3$) have three main stable phases according to temperature and pressure. At room temperature, the magnesium metasilicate crystallizes in clinoenstatite (monoclinic), which remains stable up to 700°C, the crystallizes in orthoenstatite or enstatite (orthorhombic) is stable from 700 to 1000°C, and from 1000 to 1550°C it is protoenstatite (orthorhombic) which is stable [5]. The polymorphic transformations between these phases are spontaneous and reversible. The protoenstatite form is most likely in sintered ceramics above 1000°C, but this phase is likely to turn into clinoenstatite when returning to room temperature [6]. Often other solid solutions crystallize at the same time, such as $2MgO{\cdot}SiO_2$ magnesium orthosilicate called forsterite and magnesium aluminosilicate ($2MgO{\cdot}2Al_2O_3{\cdot}5SiO_2$) known as cordierite.

The steatite ceramics are widely used in electronics, electrical engineering, radio electronics and other fields owing to their high dielectric constant which is indicative of their effectiveness in providing capacity in capacitors, on their low dielectric loss which is a measure of tendency to high-frequency circuits of which they may form a part, high electrical resistance at high temperatures and high mechanical strength [7, 8]. Such properties make it ideal for high frequency and high voltage insulation. Moreover, steatite is an excellent material to be used in electrical engineering applications as it can be readily shape-sintered into a wide variety of forms such as washers, bushings, resistor forms, spaces and beads.
Thurmauer and Rodriguez [9] concluded that a small amount of liquid was favorable to the growth of large crystals and to be the conversion to clinoenstatite. Bussem, Schusteruis and K. Stuckardt [10], reported that while the conversion is accelerated by such fluxes as Lithia, calcium fluoride, boric oxide and borax, and by large grain size, it is retarded by the presence of liquid which isolates the crystals, preventing their growth. It is generally agreed, however, that the glass phase stabilizes protoenstatite against inversion on cooling. The sintering aids were usually used to improve the sinterability of steatite ceramics made from natural material. For this purpose, B_2O_3 was used as a sintering aid due to its low melting point and less harmful effect on the insulating characteristics than other sintering aids [11, 12], B_2O_3 was commonly used as a flux for-mer and had been shown to decrease the sintering. The ac impedance analysis is a powerful means to separate out the grain boundary and grain-electrode effects, which usually are the sites of trap for defects. It is also useful in establishing its relaxation mechanism by appropriately assigning different values of resistance and capacitance to the grains and grain boundary effects.

In this paper, B_2O_3 was used to reduce the sintering temperature of steatite ceramics, and structural/micro-structural, dielectric and resistive properties of these compounds have been studied using impedance spectroscopic method to get better understanding of (i) the relaxation mechanism and (ii) microstructure-electrical properties relationship of the materials as a function of temperature and frequency.

2. Materials and Experimental Procedures

2.1. Raw material and preparation

The clay used in this study is an Algerian palygorskite, the deposit is located east of Algeria in the wilaya of Biskra, in a region known as ‹‹ Ghoufi ››. Currently the deposit is not exploited, and this study aims a valorization of this natural material.

First, the clay is stirred in a large quantity of water and then passed through a 20 micron sieve to remove the coarse particles of sand. After drying and grinding, to reduce the limestone and dolomite content, the clay is again diluted in water, the dilute hydrochloric acid is added to the clay suspension until the end of the effervescence which is caused by the release of CO_2. The suspension is left decanted and the clear water heavily loaded with Ca^+ and Cl^- ions is removed, and again distilled water is added to the clay to completely eliminate

these soluble ions. This washing operation is continued until a neutral pH is obtained. This treatment has totally eliminated calcite and dolomite.
The CaO content was completely reduced to less than 0.02 wt.%. It is clear that this treatment used is suitable for removing carbonaceous minerals from clays.

The magnesium hydroxide ($Mg(OH)_2$) is precipitated from the mixture of magnesium chloride and an ammonia solution. After total decantation of the solute, the clear water is removed and again distilled water is added to the solute. This washing operation is continued until a neutral pH is obtained. The use of precipitated Mg $(OH)_2$ strongly favors the synthesis of steatite compounds [15].

2.2. Method

The steatite (MS) compound was prepared by solid-state reaction using reagent grades powders of treated palygorskite (69 wt.%) and precipitated magnesium hydroxide (31 wt.%). These powders were stoichiometrically mixed using distilled water and zircon balls in a Teflon jar for 3 h. The mixtures MS+x wt.% B_2O_3 (with x = 0.5 and 0.75), (MSB) were prepared by mixing the powders manually in porcelain mortar. To manufacture pellets, an organic binder (polyvinyl alcohol, 5 wt.%) was manually added to the powder and disks (12.5 and 13 mm in diameter, 2 and 3 mm thickness, respectively) were shaped by uni-axial pressing under 53 MPa. The green samples were finally sintered in air at 1250°C for 2h. The crystallized phase composition has been identified by X-ray diffraction (XRD) technique using the X-ray radiation (Rigaku Mini Flex 600) and the microstructures were observed using a Scanning Electron Microscopy (TESCAN VEGA 3). The specimens were polished and electroded with a silver paste. The dielectric and electric properties were determined using HP4284A meter versus temperature (from 30 to 500°C), and the frequency range from 100Hz to 1MHz.

3. Results and Discussion

3.1. Phase Analysis and Microstructure

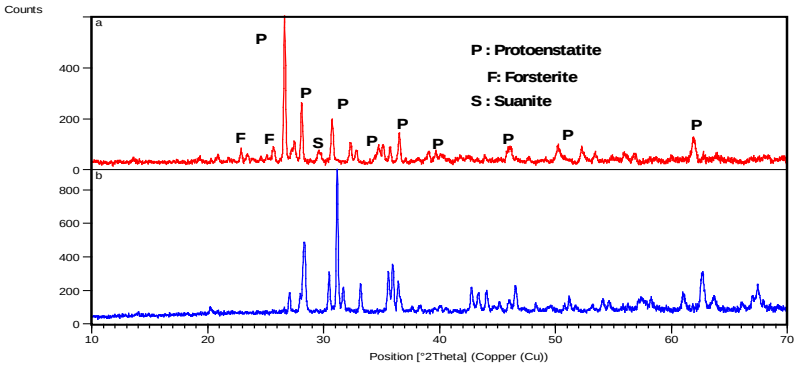

Fig. 1. X-ray diffraction of MS + x wt.% B_2O_3 compositions: (a) x= 0.5, (b) x = 0.75 sintered at 1250°C for 2h.

Fig. 1 shows the XRD results of steatite ceramics with different amounts of B_2O_3 addition. The pattern reveals the all ceramics comprised certain number of the same phases: Protoenstatite $Mg_8Si_8O_{24}$ (orthorhombic structure), forsterite ($Mg_{7.94}Si_{3.98}O_{16}$,orthorhombic structure) and Suanite ($Mg_8B_8O_{20}$, monoclinic structure).

Protoenstatite, was the most abundant mineral phase registered in the diffractograms of both steatite samples. As showed in the investigations conducted by various authors [16, 17].

The increase in the amount of B_2O_3 added induced two phenomena:

The addition of B_2O_3 from 0.5 to 0.75 % has increased the protoenstatite content from 45 to 54 % and the suanite content from 8 to 23 %.

The forsterite content decreased significantly from 22 % in the MS+0.5wt.% B_2O_3 ceramic to 6 % in the MS+0.75wt. % B_2O_3 ceramic.

These phenomena can explained as follows: upon sintering, B_2O_3 melts at approximately 480°C [18]. It then "flows" through the pores of the compacted pellets before reacting with MgO to form $Mg_8B_8O_{20}$ at approximately 750°C [19]. The subsequent reaction depends on the MgO-SiO_2 composition, i.e., either forming enstatite-group phases (1:1 MgO-SiO_2 composition ratio) or forsterite (2:1 ratio). Therefore, the presence of more B_2O_3 causes the formation of more suanite, thereby reducing the amount of MgO that can pair with SiO_2 to produce more enstatite, and Suanite is responsible for the remarkable densification and hardness improvement of the ceramics.

The density measurements performed after sintering at 1250°C for the period of 2 h showed that the MS + 0.5 wt.% B_2O_3 sample acquired 87.22 % of what can be considered as theoretical density of the natural mineral enstatite (TD = 3.21 g/cm^3). The sample MS + 0.75 wt.% B_2O_3 achieved 92.52 % of theoretical density under same conditions. The obtained densities were 2.80 g/cm^3 and 2.97 g/cm^3 for the samples MS + 0.5 wt.% B_2O_3 and MS + 0.75 wt.% B_2O_3, respectively. The densification increases with increasing B_2O_3 amount in MS.

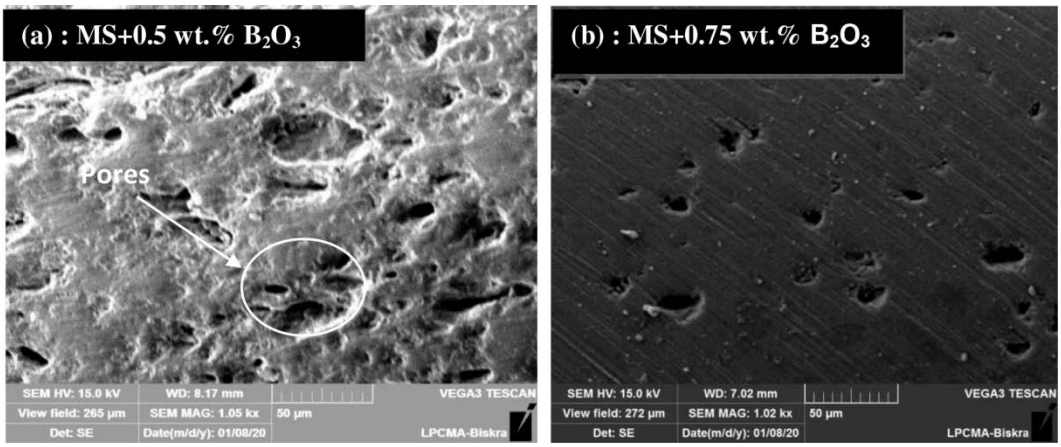

Fig. 2. Scanning electron micrographs of fracture for the sintered ceramic.

Fig. 2 shows the SEM micrographs of the MS + xwt.% B_2O_3 (with x = 0.5 and 0.75) ceramics sample. Large pores have occurred in sintered samples with 0.5 wt.% of B_2O_3 addition, and visible cracks have also formed in the steatite body. After 0.75 wt.% B_2O_3 addition, pore elimination and enhancement of densification for sample (Fig. 2(b)), were promoted by the viscous flow B_2O_3 addition and hence dense ceramic was obtained [20]. Easier densification of MS + 0.75wt.% B_2O_3 specimens may be due to the flux effect of B_2O_3 which enhances the densification during sintering. Because of the low melting point of B_2O_3, the procedure of sintering MSB ceramics would be a reactive liquid phase sintering process. With liquid formation, there was a densification, even at low sintering temperatures, due to capillary force exerted by the liquid on the particles, while actual sintering temperature was around 1400°C for steatite ceramics [11].

3.2. Dielectric studies

The dielectric constant can be defined as the ability of a material to be polarized in response to an applied electrical field. Dielectric constant or relative permittivity is the ratio of material permittivity to the permittivity of a vacuum. It represents the capacity of storage of a material. The more polarized is the material in the presence of an electrical field the more it will show a high dielectric constant $\varepsilon_r = \varepsilon/\varepsilon_o$.

Where ε_r is the relative permittivity, ε is the permittivity of the dielectric medium, and ε_0 is the permittivity of a vacuum.

All glass-ceramics exhibit a normal dielectric dispersion, due to Maxwell-Wagner type interfacial polarization in accordance with Koop's phenomenological theory [21, 22] and that can be attributed to the decrease of dielectric constants with increasing frequency. This theory says that the conductivity of grain boundaries contributes more to the dielectric constant at lower frequencies. The dielectric properties are due to combined intrinsic and extrinsic factors: lattice vibration modes, porosity, chemical homogeneity, oxygen vacancies, grain size [23]. Domination of any of these factors varies with the sample's composition and sintering temperature [24].

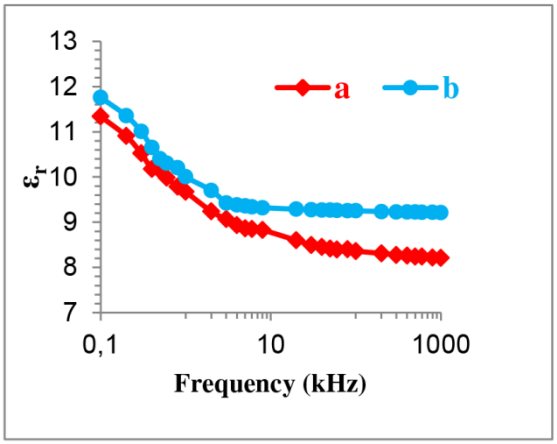

Fig. 3. Variation of dielectric constant (ε_r) with frequency at room temperature of MS +x wt.% B_2O_3 compositions: (a) x = 0.5 and (b) x = 0.75.

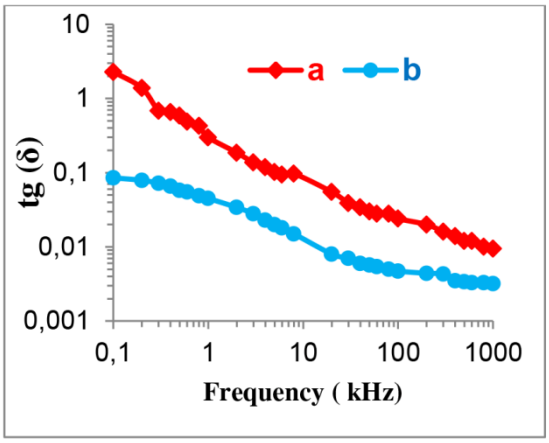

Fig. 4. Variation of loss tangent (tgδ) with frequency at room temperature of MS +x wt.% B_2O_3 compositions: (a) x=0.5 and (b) x = 0.75.

Figs. 3 and 4 shows the variation of relative dielectric constant (ε_r) and loss tangent (tgδ) of MS + x wt.% B_2O_3 ceramics, respectively with frequency at room temperature. It can be observed that dielectric constants and losses first decrease with increasing frequency and then reach almost constant values at high frequencies. According to the Maxwell-Wagner model, this variation occurs because the hopping between different metal ions cannot follow the alternating field because of the predominance of species such as lattice defects, oxygen vacancies, grain size/boundary and secondary phases [25].

The introduction of B^{3+} cations in MS system could generate oxygen vacancies in the glass structure, and thus, the dielectric behaviour is not intrinsic in character and may be induced by structure defects. Hence, MSB ceramics exhibit space charge polarization, which is thought to be arising from the difference between the grain boundaries conductivity of various phases. This causes a build-up of charge carriers at the interface, which corresponds to a high value of dielectric constant, from 8.209 for MS + 0.5 wt.% B_2O_3 to 9.214 for MS + 0.75 wt.% B_2O_3 at 1 MHz.

The charge carrier's accumulation at the grain boundaries is responsible for higher values of dielectric constant at low frequencies [26]. At high frequency, ε_r results from the grains which have a small dielectric constant [27].

There was also a report on the effect of density, which is inversely proportional to porosity, on the dielectric constant of ceramics [28]. A denser ceramic exhibits a higher grain boundary density and hence a higher dielectric constant [29, 30]. It is then argued that the main cause of the vast increase in εr in the B_2O_3-added steatite ceramics was the excellent densification of the ceramics.

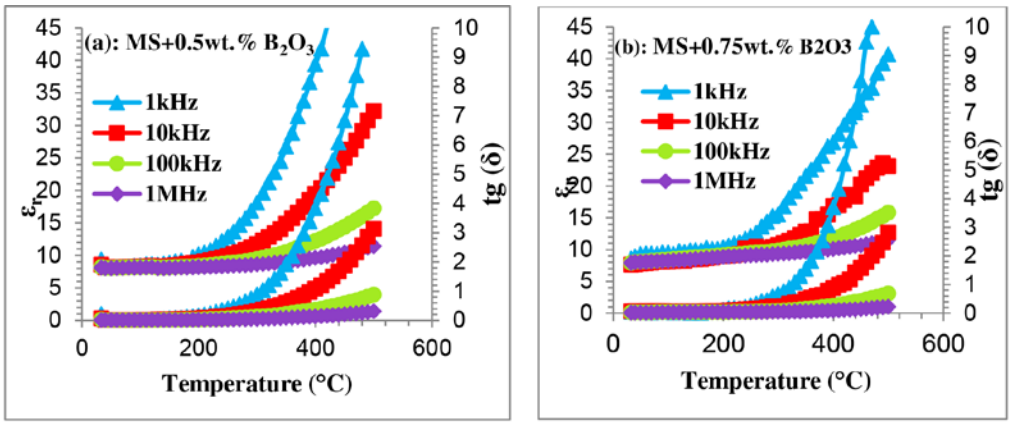

Fig. 5. Temperature dependence of permittivity and dielectric loss at different frequency of MS +x wt.% B_2O_3.

Fig. 5 shows the temperature dependence of the dielectric constant (ε_r) and dielectric losses tangent (tgδ) of MS + x wt.% B_2O_3 ceramics at different frequencies (1 kHz, 10 kHz, 100 kHz and 1 MHz). The increase in permittivity at higher temperatures is possibly due to the polarizability of K^+ ions (3.83Å), which is higher than that of Mg^{+2} ions (1.32 Å). Steatite exhibits interfacial or space charge polarization arising from the differences amongst the conductivity of phases, which are present in the material. If phases of different conductivity occur readily through present, the motion of charge carriers one phase, but it is interrupted when it reaches a phase boundary of other phases. This causes a build-up of charge at the interface, which corresponds to a large polarization and high value of dielectric constant. The charge accumulation at the grain boundaries is responsible for higher values of dielectric constant at low frequencies [31,32]. At high frequencies, ε_r results from the grains which have

a small dielectric constant [17]. It is interesting to note that as the temperature increases, the dielectric constant increases at all frequencies.

The dielectric loss increase rapidly at higher temperature this may be due to the rapid increase of conductivity of the material. The rapid increase of loss tangent at higher temperature in low frequency region may be due to space charge polarization. In addition, the high loss factor of steatite at higher temperatures is due to the glass content and the high mobility of alkali ions (K^+). Note is made that for MS+0.75 wt.% B_2O_3 even at high frequencies (1 MHz) and temperature (500°C), the dielectric loss (tgδ) remains relatively low (0.214), an important fact from the point of view of technological applications such as: electronics, electrical engineering, radio electronics, halogen bulb holders, NH-fuses, element formers and casings for thermostats.

3.3. Complex impedance spectrum analysis

The complex impedance spectroscopic (CIS) technique is used to analyze the electrical response of polycrystalline samples in a wide range of frequencies and temperatures. This technique is based on the application of an alternating voltage signal to a sample and the measurement of the corresponding phase shifted current response. The complex impedance spectroscopy is a powerful tool to analyze the microstructure and properties relationship of the material.

The physical process occurring inside the sample can be modeled as an equivalent circuit using impedance spectra. The electrical AC response of the material may be represented in any of the four basic formalisms via complex permittivity (ε^*), complex impedance (Z^*), complex admittance (Y^*) and complex electric modulus (M^*), which are interrelated to each other [33]. These relations offer a wide scope for a graphical analysis of the various electrical parameters under different experimental conditions (temperature and frequency). From the microstructural point of view, a ceramic sample is composed of grains and grain boundaries, exhibiting different resistivity (ρ) and dielectric permittivity (ε). The real part (Z') and the imaginary part (Z'') of the complex impedance are given by the following equations [34]:

$$Z' = R_g/(1 + (\omega R_g C_g)^2 + R_{gb}/(1 + (\omega R_{gb} C_{gb})^2) \quad (1)$$

$$Z'' = \omega R_g^2 C_g/(1 + (\omega R_g C_g)^2) + \omega R_{gb}^2 C_{gb}/(1 + (\omega R_{gb} C_{gb})^2) \quad (2)$$

where, R_g and C_g are the resistance and capacitance of the grain, while R_{gb} and C_{gb} are the resistance and capacitance of the grain boundary, respectively.

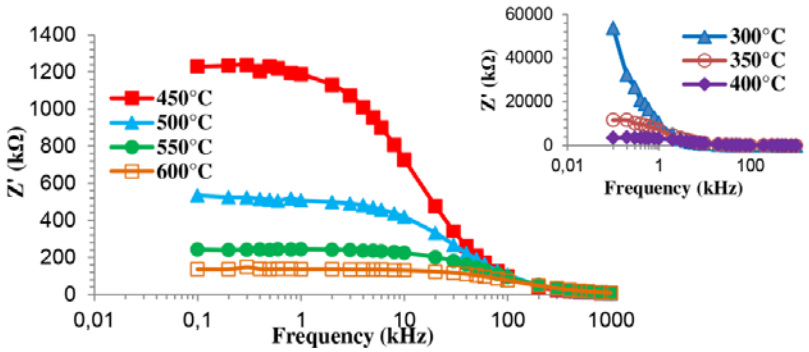

Fig. 6. Variation of real part of impedance (Z') with frequency at different temperature of MS + 0.75 % B_2O_3.

Fig. 6 shows the variation of the real part of impedance (Z') with frequency at different temperatures for MS + 0.75 wt.% B_2O_3 specimens. It is observed that the magnitude of Z' decreases with increasing of the frequency and temperature, indicating an increase in ac conductivity. The Z' values for all temperatures merge at high frequencies (> 10 kHz), which indicates the release of space charges. This may be attributed to the increase of ac conductivity with temperature and frequency in the higher frequency region due to the removal of space charge as a result of reduction in potential barrier height [35]. Furthermore, at low frequency, Z' values decrease with an increase in temperature and reveal negative temperature coefficient of resistance (NTCR) behavior similar to that of semiconductors.

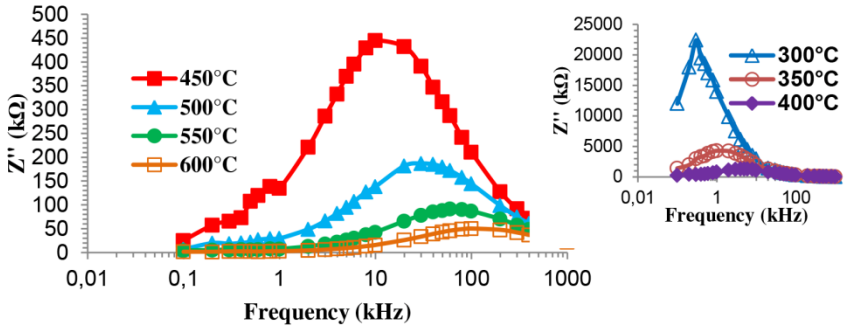

Fig. 7. Variation of imaginary part (Z'') of impedance with frequency at different temperature of MS + 0.75% B_2O_3.

Fig. 7 shows the variation of imaginary part (Z'') with frequency and temperature. As the temperature increase, the obtained peaks are more and more flattened in this specimen indicating relaxation is stronger at higher temperatures. It can be seen that the curves display broad and intensity peaks with asymmetrical shape. The broadening of the peak and half-widths of the peaks indicate multiple relaxations and deviations from Debye behavior [36]. The average peak position regularly changes towards the higher frequency side on increasing temperature. Furthermore, as the temperature increases, the magnitude of Z'' decreases and the effect is more pronounced at the peak position. The shift of the peaks towards higher frequency on increasing temperature is due to the reduction in the bulk resistivity.

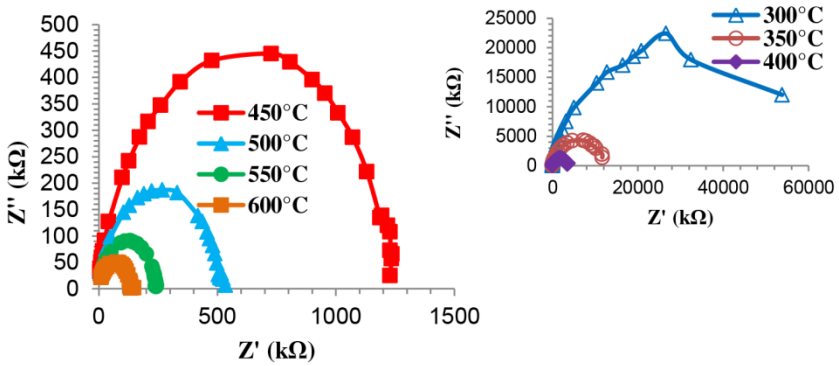

Fig. 8. Complex impedance plots (Z'' versus Z') of MS + 0.75 % B_2O_3 at different temperature.

Fig. 8 shows Cole-Cole plots (Z'' versus Z') for MS + 0.75 % B_2O_3 at various temperatures. For temperature measurements below 350°C, there is no semicircle formation. By increasing temperature, the Z'' versus Z' curve changes and semicircles appear indicating

an increase of the materials conductivity. The presence of a single semicircular arc passing through the origin in the entire frequency region for all the temperatures indicates that the relaxation mechanism in MSB may be only a grain effect. Hence it is appropriate to fit the Z-plot to a single R_gC_g parallel circuit due to the fact that the response peaks of the grain boundaries are not present. The expression for Z^* is given by:

$$Z^* = Z' + i\,Z'' = R_g/(1 + i\omega\, R_g\ C_g) \qquad (3)$$

where, R_g and C_g are the grain resistance and grain capacitance, respectively. Unfortunately, Eq. (3) cannot be used to describe the experimental data very well due to the depressed nature of the semicircular arcs. Furthermore, for Debye type relaxation, one expects semicircular plots with the center located on the Z'-axis, whereas for a non-Debye type relaxation these Argand plane plots are close to semicircular arcs with end points on the real axis and the center lies below this axis. The complex impedance in such a case can be described as [37]:

$$Z^*(\omega) = Z' + iZ'' = R/(1 + (i\omega/\omega_0)^{1-\alpha}) \qquad (4)$$

where, α represents the magnitude of the departure of the electrical response from an ideal condition and this can be determined from the location of the center of the semicircles.
Further, it is known that when α approaches to zero, i.e., {(1-α) = 1}, Eq. (4) gives rise to classical Debye's formalism. It can be seen from the impedance plots (Fig. 8) that the curves are not full semicircle, they are depressed one, i.e., center of semicircles lie little below the abscissa (Z') axis (α > 0), which increases with the rise in temperature suggesting the dielectric relaxation to be non-Debye type in MSB composition.

The value of grain resistance and capacitance are listed in Table I.

Tab. I Grain resistance and capacitance obtained from Nyquist plot (Z'' vs Z').

T (^{o}C)	MS + 0.5 wt.% B_2O_3		MS + 0.75 wt.% B_2O_3	
	R_g (Ω)	C_g (F)	R_g (Ω)	C_g (F)
300	31024676	1.28314E-11	26614000	1.99438E-11
350	6437254	4.12276E-11	7176000	2.219E-11
400	1647058	3.22263E-11	1714000	1.85806E-11
450	358866	2.2186E-11	477561	1.66718E-11
500	191004	2.77892E-11	267759	1.98233E-11
550	105321	2.51985E-11	132620	2.00115E-11
600	57717	3.44863E-11	76205	2.08957E-11

The grain boundary resistance decreases with rise in temperature; this may be due to the increase of the material conductivity.

3.4. Electrical Modulus Spectrum Analysis

Complex electric modulus formalism/analysis give information on the nature of polycristalline (homogeneous or inhomogeneous) samples, which can be resolved into bulk and grain boundary effects. It indicates also the electrical phenomenon with the smallest

capacitance occurring in a dielectric system [38]. The advantage of adopting complex electric modulus formalism is that it can discriminate electrode polarization from grain boundary conduction process. In polycrystalline materials, impedance formalism might emphasize grain boundary conduction process, while bulk effects on frequency domain would dominate in the electric modulus formalism. The use of modulus spectroscopy plot is particularly useful for separating components with similar resistance but different capacitance. The other advantage of electric modulus formalism is that the electrode effect is suppressed. Due to the above reasons, the complex electric modulus (M^*) have been calculated from the impedance data using the following relation:

$$M^*(\omega) = 1/\varepsilon(\omega) = M' + jM'' \quad (5)$$
$$M' = \omega C_0 Z'' \quad and \quad M'' = \omega C_0 Z'$$

where, ω is the angular frequency ($2\pi f$), $C_0 = \varepsilon_0 (A/t)$ is the geometrical capacitance, ε_0 is the permittivity of free space, A is the area of the electrode surface and t is the thickness of the sample.

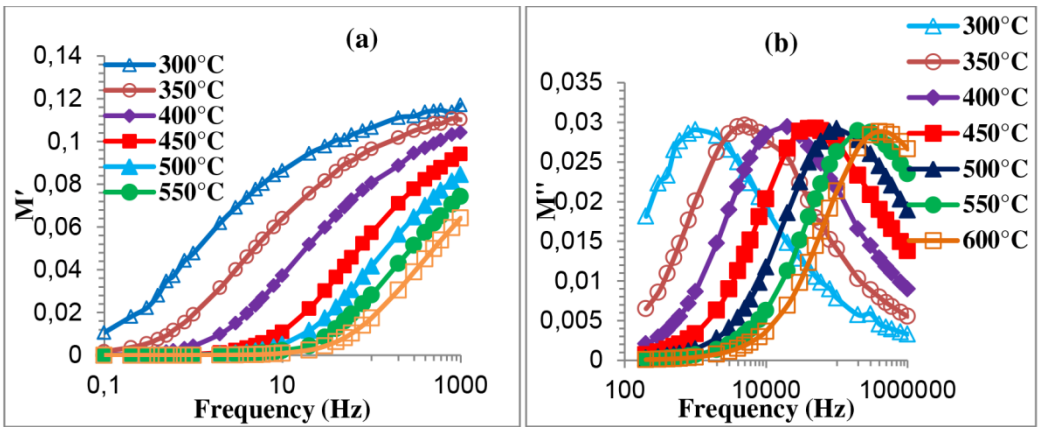

Fig. 9. Variation of (a) M' and (b) M'' with frequency of MS + 0.75 wt.% B_2O_3.

Fig. 9(a) shows the variation of M' with frequency of MS + 0.75 wt.% B_2O_3 at various temperatures. A very low value (~zero) of M′ in the low frequency region is observed. Continuous increases in the dispersion with increasing frequency for all the temperatures are observed. Such observations could possibly be related to lack of restoring force governing the mobility of the charge carriers under the action of an induced electric field. This confirms the elimination of electrode effect in the material. The value of M' decreases with the rise in temperature in the high frequency region. Fig. 9(b) shows the variation of M'' with frequency over a wide temperature range and frequencies ascribing correlation between motions of mobile ions [39]. A well-defined relaxation mechanism is observed in temperature range 300-500°C. The relaxation peaks shift towards higher frequency side with the rise in temperature. The frequency region below peak maximum (M'') represents the range in which the charge carriers are mobile at long distances. At frequencies above peak maximum, the carriers are confined to potential wells and are mobile at short distances [40]. The nature of modulus spectrum suggests the existence of hopping mechanism of electrical conduction in the material. The value of M'' increases as a function of temperature.

3.5. Electrical Conductivity Analysis

The conductivity data were obtained using the following relation [41]:

$\sigma_{ac} = \varepsilon_0 \varepsilon'' \omega$ (6)

where ε_0 is the permittivity of vacuum, ε'' the imaginary part of the dielectric constant and ω is the angular frequency.

ε'' is calculated by using the following formula:

$$\varepsilon'' = \frac{Z'}{\omega C_0 (Z'^2 + Z''^2)} \quad (7)$$

where $C_o = \varepsilon_o \cdot A/t$, t and A are the thickness and area of the electrode, respectively.

Finally, the ac conductivity was obtained according to the equation:

$\sigma_{ac} = Z' t/(Z'^2 + Z''^2) A$, ($\Omega^{-1}$/m).

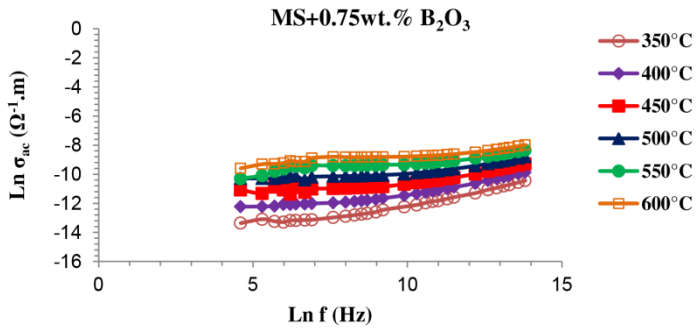

Fig. 10. Frequency dependence of ac conductivity vs frequency at different temperatures.

Fig. 10 shows the plot of ac conductivity versus frequency at different temperatures of MS + 0.75 wt.% B_2O_3 ceramics. The frequency dependence of the material conductivity exhibits both low and high frequency dispersion phenomena. But it can be observed that the dispersion is more important at low frequency, the ac conductivity of the materials obeys the Jonschers's power law equation [42] given by:

$$\sigma(\omega) = \sigma_{dc} + A\omega^n \quad (8)$$

where, n is the frequency exponent in the range of 0<n<1, A and n are thermally activated quantities, hence electrical conduction is thermally activated process. The origin of the frequency dependence of conductivity lies to the relaxation phenomena arising due to mobile charge carriers. When the mobile charge carriers hops to a new site from its original position, it remains in a state of displacement between two potential energy minima, which includes contributions from other mobile defects. After a sufficiently long time, the defect could relax until the two minima in lattice potential energy coincide with the lattice site. The values of exponent n, σ_{dc} and A were obtained by fitting Eq. (6) (σ_{ac} versus ω) at different temperatures. The fit quality is usually evaluated by comparing the squared coefficient of linear correlation coefficient (R^2) obtained for each temperature (see Table II). It can be seen that the value of n is always less than 1 and decreases when temperature increases. The model based on hopping of charge carriers over potential barrier, [43] predicts a decrease of the (n) index with the increase in temperature and hence this is consistent with the experimental results. Therefore, the conduction in the system may be considered to be due to the short-range translational type hopping of charge carriers. This indicates that the conduction process is a thermally activated process. Hopping conduction mechanism is generally consistent with the existence of a high density of states in the materials having bandgap similar to that semiconductor.

The *dc* (bulk) conductivity, σ_{dc} of the sample has been evaluated from the impedance spectrum using the relation $\sigma_{dc} = t/AR_b$ where R_b is the bulk resistance (obtained from the

intercept of the semicircular arcs Z'' on the real axis (Z')), t the thickness and A the surface area of the sample.

Tab. II The fitting parameters obtained from experimental data of the conductivity as function of frequency (σ_{ac} versus ω) using the Jonscher' power law.

T (°C)	σ_{dc} (Ω^{-1}.m)	A	n	R^2
300	$3.449.10^{-6}$	$6.586.10^{-3}$	0.398	0.936
350	$1.589.10^{-5}$	$1.231.10^{-7}$	0.329	0.951
400	$5.336.10^{-5}$	$1.131.10^{-2}$	0.263	0.930
450	$1.509.10^{-4}$	$1.739.10^{-2}$	0.204	0.868
500	$3.469.10^{-4}$	$2.695.10^{-2}$	0.155	0.848
550	$7.666.10^{-4}$	$2.290.10^{-2}$	0.150	0.876
600	$1.365.10^{-3}$	$2.615.10^{-2}$	0.131	0.914

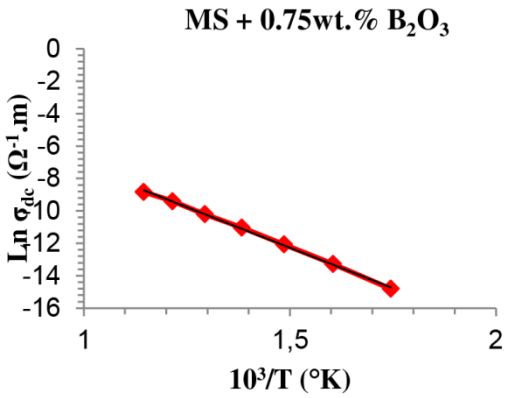

Fig. 11. Variation of $ln\sigma_{dc}$ with 10^3/T.

Fig. 11 shows the variation of $ln\sigma_{dc}$ with 10^3/T. It is observed that σ_{dc} increases with the increase in temperature further confirming the NTCR behavior. The nature of variation is linear and follows the Arrhenius relationship:

$$\sigma_{dc} = \sigma_0 \, exp\,(E_a/k_b\,T) \qquad (9)$$

where, E_a is the activation energy of conduction and T the absolute temperature, k_B is Boltzmann constant and σ_0 is the pre-exponential factor. The value of activation energy (E_a) as calculated from the slope of $ln\sigma_{dc}$ with 10^3/T curve is found to be 0.86 eV. Such a value of activation energy indicates that the conduction mechanism of studied system may be due to the polaron hopping based on electron carriers.

Fig. 12 shows the variation of relaxation time ($ln\tau$) with inverse of absolute temperature (10^3/T). The characteristic relaxation time (τ) was calculated from Z'' and M'' vs. frequency plots using the relation: $\tau = 1/\omega = 1/2\pi f_{max}$, where f_{max} is the relaxation frequency (frequency at which Z'' or M'' was found to be maximum). The logarithmic of the

relaxation times derived from Z″ vs. frequency and M″ vs. frequency functions, as function of reciprocal temperature 1/T are shown in Fig. 12. The data are described by Arrhenius' expression:

$\tau_{Z''} = \tau_{0Z''} \, exp\,(E_{a1}/k_B\,T)$, (10)

$\tau_{M''} = \tau_{0M''} \, exp\,(E_{a2}/k_B\,T)$, (11)

where, E_{a1} and E_{a2} are the activation energies for the conduction relaxation derived from $Z^{''}$(f) and $M^{''}$(f) functions, where $\tau_{0Z''}$ and $\tau_{0M''}$ are the pre-exponential factor or characteristic relaxation time constants, respectively. A near value for E_{a1} and E_{a2} is observed on the entire range of temperature measurements being equals to 0.85 and 0.84 eV, respectively. This value of E_a is approximately the same as the energy required (1 eV) for motion of oxygen vacancies [44]. This confirms that the observed conductivity is due to the movements of oxygen vacancies in the material.

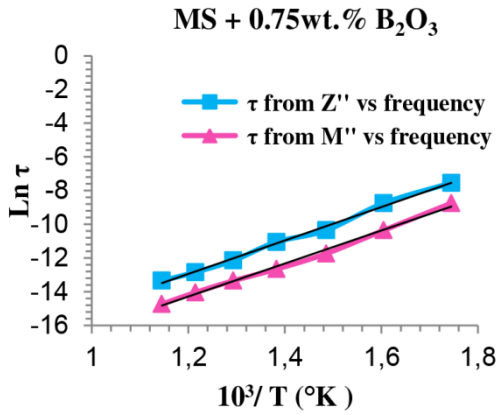

Fig. 12. Arrhenius diagram of relaxation times, $ln(\tau_{Z''})$ and $ln(\tau_{M''})$ as a function of reciprocal temperature.

4. Conclusion

Preliminary structural and detailed dielectric and electrical properties of B_2O_3 added steatite (named MSB) ceramics were studied. The XRD patterns reveal protoenstatite, was the most abundant mineral phase for the different studied compositions. The dielectric constant increases with increasing B_2O_3 amount in MS, it goes from 8.209 for MS + 0.5 wt.% B_2O_3 to 9.214 for MS + 0.75 wt.% B_2O_3. Impedance analysis (Nyquists plots) shows bulk effect to be dominant in electrical behavior of MS + 0.75 wt.% B_2O_3 which is again confirmed in modulus formalism. It shows that the compound exhibit negative temperature coefficient of resistance (NTCR) type behavior usually found in semiconductors. The activation energy (E_a) of the compound under investigation is calculated using the arrhenius expression (derived from Z″ (*f*) and M″ (*f*) functions). The activation energy (E_a) of the compound the value of activation energy (E_a) as calculated from the slope is found to near 1 eV, this value is due to the movements of oxygen vacancy in the material.

5. References

1. A. Terzić, Lj. Andrić, J. Stojanović, N. Obradović, M. Kostović, Mechanical activation as sintering pre-treatment of talc for steatite ceramics, Sci. Sinter. 46 (2) (2014) 247-258.

2. H. S. Soykan, Low-temperature fabrication of steatite ceramics with boron oxid addition, Ceramics International, 33 (2007) 911-914.
3. Hassan Gokçe et al, Characterization of microstructural and thermal properties of steatite/cordierite ceramics prepared by using natural raw materials, Journal of the European Ceramic Society, Vol. 31, 14, (2011) 2741-2747.
4. E. A. Takher, T. I. Feoseeva, V. Y. Kellerman, R. Popilskii, Glass and Ceramics. 31 (1974) 108.
5. R. Joseph, Smyth, Experimental Study on the polymorphim of Enstatite, American Mineraolgy, Vol. 56 (1974) 345-352.
6. W. Mielcarek, D. Nowak-Wozny, K. Prociow, Correlation between $MgSiO_3$ phases and mechanical durability of steatite ceramics, J. Eur. Ceram. Soc. 24 (15/16) (2004) 3817-3821.
7. W. D. Kingery, H. K. Bowen, D. R. Uhlmann, Introduction to Ceramics, Wiley & Sons, New York, (1976) 307.
8. A. K. Kukarni, P. Y. Dalvi, M. L. Barde, Trans of Powder Metallurgy Assoc of India 17 (1990) 101.
9. H. Thurnauer, A. R. Rodriguez, Notes on the constitution of steatite. Journal of the American Ceramic Society, 25(15) (1942) 443-450.
10. W. Bussem, C. Schusterius, K. Stuckardt, "Con- stitution of Steatite: 11, Glass Phase," Verofent. Kaiser- Wilhelm Inst. Silikatforsch. Berlin-Dahlem, 9, 64 (1938) ; Wiss. Verijfeent. Siemens- Werken, 17 [l] 59-77 (1938); Ceram. Abs., 18 [4] 110 (1939).
11. K. Sumi, Y. Kobayashi and E. Kato, Low-temperature fabrication of cordierite ceramics from kaolinite and magnesium hydroxide with boron oxide additions››, Journal of American Ceramic Society, Vol. 82, No. 3 (1999) 783-785.
12. L. H. Luo, H. Zhou, XuC. J. Mat. Elec. 12, (2001) 371.
13. C. L. Huang, J. J. Wang, B. J. Li, W. C. Lee, J. Al-loy. Compd, 461 (2008) 440.
14. H. F. Zhou, H. Wang, D. Zhou, L. X. Pang and X. Yao, Mater. Chem. Phys, 109, (2008) 510.
15. Y. Kobayashi, K. Sumi, E. Kato, Preparation of dense cordierite ceramics from magnesium compounds and kaolinite without additives, Ceramics International 26 (2000) 739-743.
16. J. Jiao, X. Liu, W. Gao, C. Wang, H. Feng, X. Zhao, L. Chen, Material Research Bulletin, 45 (2010) 181.
17. P. Ptácek, K. Lang, F. Soukal, T. Opravil, E. Bartonícková, L. Tvrdík, Journal of European Ceramic Society (2014) 515.
18. S.-F. Wang, Y.-R. Wang, Y.-F. Hsu, C.-C. Chuang, Effect of additives on the thermal properties and sealing characteristic of BaO-Al_2O_3-B_2O_3-SiO_2 glass-ceramic for solid oxide fuel cell application, Int. J. Hydrogen Energy, 34 (2009) 8235-8244.
19. A. Üçyıldız, İ. Girgin, Controlled synthesis, characterization and thermal properties of $Mg_2B_2O_5$, Cent. Eur. J. Chem. 8, 4 (2010) 758-765.
20. J. C. Anderson, Dielectrics. Chapman and Hall, London (1964).
21. R. B. Hilborn Jr., Maxwell-Wagner Polarization in Sintered Compacts of Ferric Oxide, J. Apll. Phys. 36 (1965) 1553-1557.
22. C. G. Koops, On the dispersion of resistivity and dielectric constant of some semiconductors at audio frequencies, Phys. Rev. 83 (1951) 121-124.
23. I. Choi, Y. Cho, Effects of various oxide fillers on physical and dielectric properties of calcium aluminoborosilicate based dielectrics, J. Electroceram. 23(2) (2009) 185-190.
24. R.N. Singh, J.P. Singh, B. Lal, A. Singh, Preparation and characterization of nano spinels for electrocatalysis of oxygen evolution in alkaline solutions, Int. J. Hydrogen

Energy 32 (2007) 11-16.
25. C. L. Huang, C. S. Hsu, Improved high Q value of $0.5LaAlO_3$-$0.5SrTiO_3$ microwave dielectric ceramics at low sintering temperature, Mater. Res. Bull. 36 (2001) 2677-2687.
26. A. Prasad, A. Basu, Dielectric and impedance properties of sintered magnesium aluminum silicate glass-ceramic, J. Adv. Ceram. 2(1) (2013) 71-78.
27. K. Jawahar, R.N.P. Choudhary, Structural, thermal and dielectric properties of $La_3/2Bi_3/2Fe_5O_{12}$, Solid State Commun. 142 (2007) 449-452.
28. V. R. K. Murthy, S. Sundaram, B. Viswanathan, Microwave Materials, Springer, (1994).
29. P. Lunkenheimer, V. Bobnar, A. V. Pronin, A. I. Ritus, A. A. Volkov, A. Loidl, Origin of apparent colossal dielectric constants, Phys. Rev. B. 66 (2002) 052105.
30. G. Zang, J. Zhang, P. Zheng, J. Wang, C. Wang, Grain boundary effect on the dielectric properties of $CaCu_3Ti_4O_{12}$ ceramics, J. Phys. D: Appl. Phys. 38 (2005) 1824-1827.
31. K. Jawahar, RNP. Choudhary, Structural, thermal and dielectric properties of $La_3/2Bi_3/2Fe_5O_{12}$, Solid State Commun, 142 (2007) 449-452
32. YJ. Hsiao, YH. Chang, TH. Fang et al, Dielectric relaxation properties of perovskite-pyrochlore biphase ceramics, Appl Phys Lett, 87 (2005) 14290.
33. I. M. Hodge, M. D. Ingram and A. R. West, Impedance and modulus spectroscopy of polycrystalline solid electrolytes, J. Electroanal. Chem., 74 (1976) 125.
34. J. R. Macdonald, Impedance Spectroscopy, Wiley, New York, (1987).
35. K. Lily, K. Kumari, K. Prasad and R.N.P. Choudhary, J. Alloys Compd., 453 (2008) 325.
36. Y. M. Li, R. H. Liao, X. P. Jiang and Y. P. Zhang, J. Alloys Compd., 484 (2009) 961.
37. J. Liu, C. Duan, W. N. Mei, R. W. Smith and J. R. Hardy, Dielectric properties and Maxwell-Wagner relaxation of compounds $ACu_3Ti_4O_{12}$, Journal of Applied Physics., 98 (9) (2005) 093703.
38. F. A. Kroger and H.J. Vink, Relation between the concentrations of imperfections in crystalline solids, Solid State Phys. 3 (1956) 307.
39. F. Borsa, D. R. Torgeson, S. W. Martin, et al, Relaxation and fluctuations in glassy fast-ion conductors: Wide-frequency-range NMR and conductivity measurements Phys, Rev. B, 46 (1992) 795-800.
40. B. Behera, P. Nayak, R. N. P. Choudhary, Mat. Res. Bull., 43 (2008) 401.
41. H. M.Zeyada, F. M. El-Taweel, M. M. El-Nahass, M. M. El-Shabaan, Effect of substitution group on dielectric propertiesof 4H-pyrano [3, 2-c] quinoline derivatives thin films, Chinese Physics B, vol. 25, no. 7 (2016) 077701
42. A. K. Jonscher, the Universal Dielectric Response. Nature, 267 (1977) 673.
43. S. R. Eilliot, Temperature dependence of ac conductivity of calcogenide glasses, Philosophical Mag. B, 37 (1978) 553.
44. S. Sen, R. N. Choudhary, P. Paramanik, Structural and electrical properties of Ca^{2+} modified par PZT electro ceramics, Physica B: Condensed Matter, 387 (2007) 56.

Сажетак: *B_2O_3 је коришћен за смањење температуре синтеровања стеатитне (назване МСБ) диелектричне керамике. Електрична својства ове композиције су проучавана коришћењем спектроскопске методе импедансе да би се боље разумели електрична проводљивост, механизам диелектричне релаксације и однос микроструктура-електрична својства материјала у функцији температуре и фреквенције. Ови узорци су припремљени техником реакције у чврстом стању и њихово једнофазно формирање је потврђено техником дифракције рендгенских зрака. Спектроскопске студије диелектричне и комплексне импедансе спроведене су у*

широком фреквентном (102-106 Hz) и температурном опсегу (30-500°C). Диелектричне константе се смањују са повећањем фреквенције за сваки узорак, а затим се стабилизују на фреквенцијама нижим од 100 kHz. Диелектрична константа се повећава са додатком B_2O_3. Природа фреквентне зависности наизменичне проводљивости МСБ следи Јоншеров закон снаге, а израчуната једносмерна проводљивост прати Ариниусово понашање. Најквистов дијаграм (Z″ vs Z′) је открила присуство само ефекта границе зрна од 350°C надаље. Појава појединачног лука у комплексном модулу спектра МСБ композиција потврђује монофазне карактеристике, а такође потврђује присуство недебајевског типа вишеструких релаксација у материјалу.

***Кључне речи**: Палигорскит, стеатит, B_2O_3, диелектрична својства, АЦ импендансна спектроскопија.*